ISCI, Volume *15*

Supplemental Information

A Moisture-Penetrating Humidity Pump Directly Powered by One-Sun Illumination

Biye Cao, Yaodong Tu, and Ruzhu Wang

Figure S1

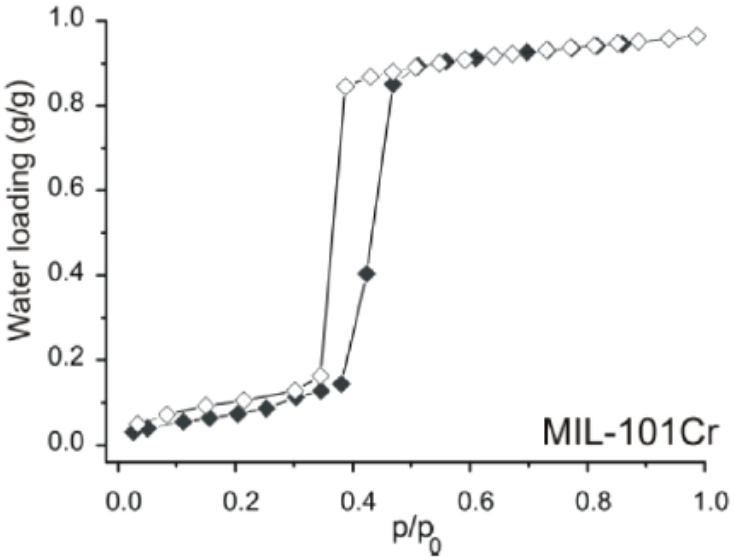

Figure S1. The water adsorption isotherm of pure MIL-101(Cr) measured by A. Khutia et. al.(Khutia et al., 2013) Closed and open marks represent the adsorption and desorption processes, respectively. Related to Figure 2.

Fig. S2.

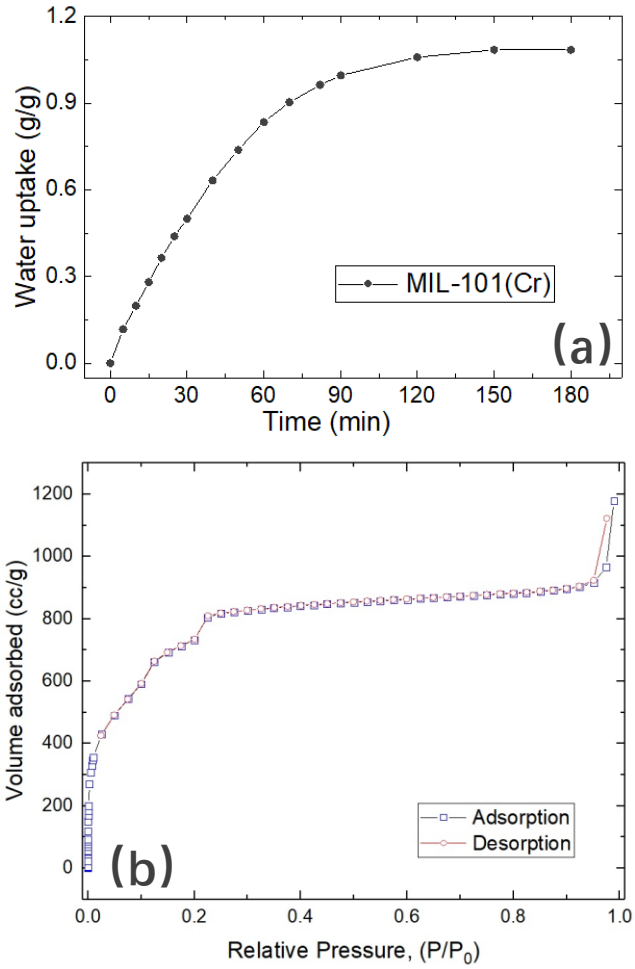

Figure S2. Dynamic water adsorption of MIL101(Cr) (a) and nitrogen adsorption test (b). The dynamic water adsorption as well as the nitrogen adsorption test of the MIL101(Cr) were carried out to evaluate the quality of the MOF we prepared. The dynamic adsorption (a) was carried out at 25℃, 70%RH and a final water uptake of 1.08g/g is obtained. From the nitrogen adsorption (b) result, the BET surface area can be calculated as 2906 m^2/g. Related to Figure 2.

Fig. S3.

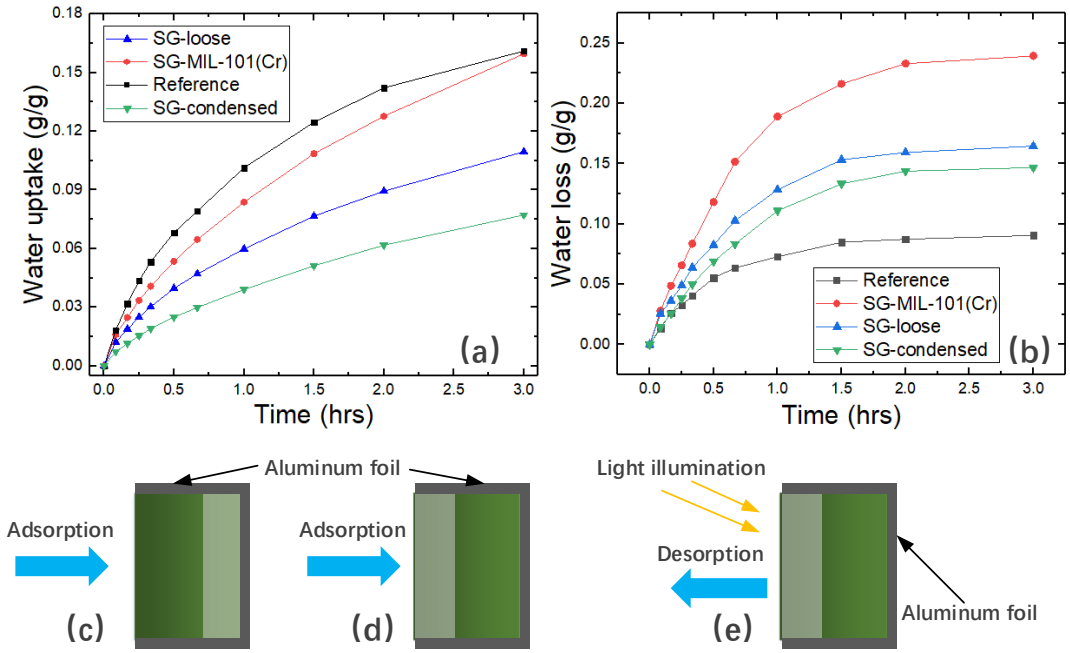

Figure S3. The dynamic adsorption(a) and desorption(b) curves. To completely meet the real working conditions, all the adsorption measurements were carried out with the process shown in (c) while (d) stands for the curve SG(reference). All the desorption measurements were taken using the setup (e). Related to Figure 2 and Table 1.

Fig. S4.

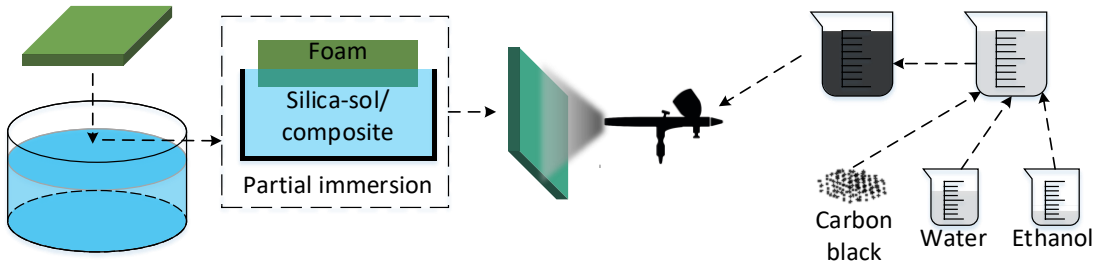

Figure S4. Fabrication steps of moisture permeable panel. The volume ratio of water and ethanol applied for CB suspension is 3:1. In the partial immersion, the liquid is either silica-sol or the composite of silica-sol and MIL101(Cr) suspension. Related to Figure 1.

Fig. S5.

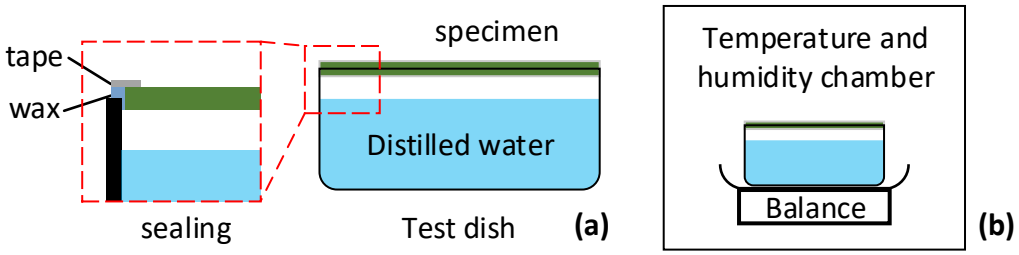

Figure S5. Apparatus of Water Vapor Transmission test. (a) specimen attachment and sealing details. Wax is used as sealant and tapes cover the wax as insurance. (b) the apparatus should be placed in a temperature and humidity chamber to control the surrounding environment. Related to Figure 2.

Fig. S6

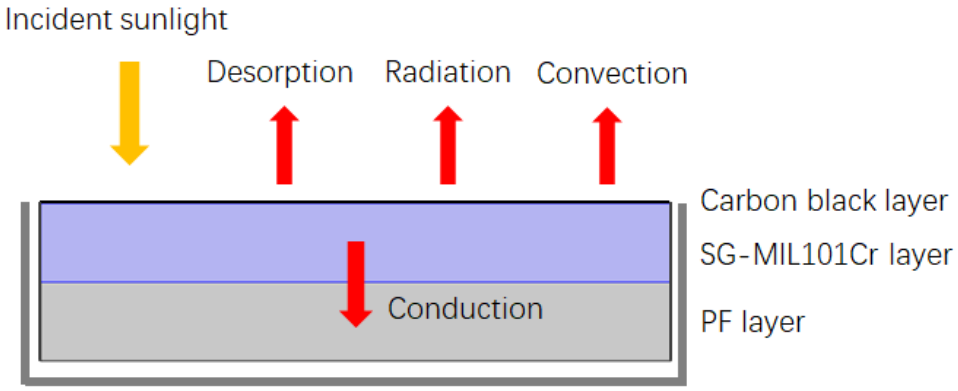

Figure S6. The heat transfer model during desorption stage. Related to Figure 3 and Figure 6.

Fig. S7

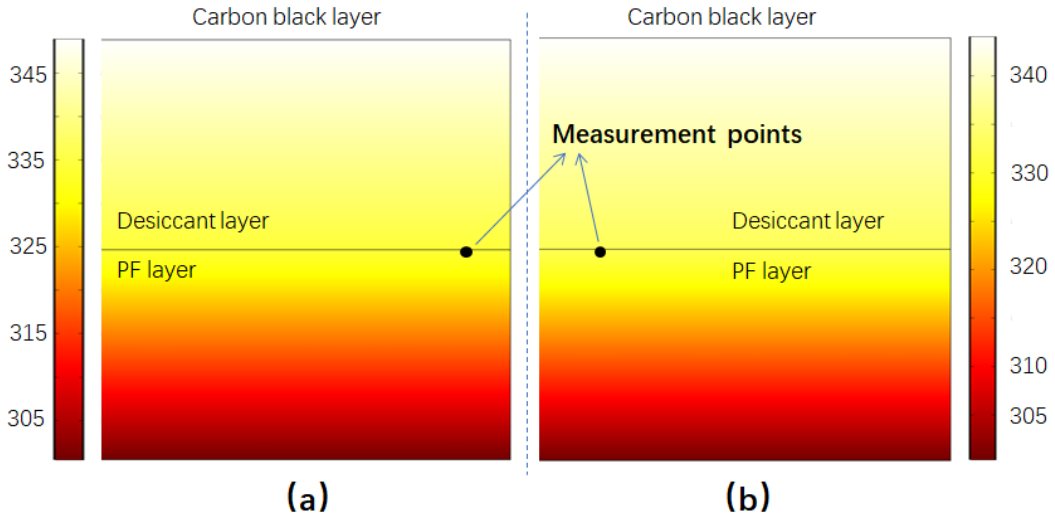

Figure S7. Simulation of temperature profile with dry (a) and wet (b) desiccant layers. Two measurement points are selected on the interface between the desiccant layer and the PF layer. Related to Figure 3 and Figure 6.

Table S1. Gluing amount of different kinds of moisture permeable panels. Related to Figure 2.

Panel description	SG-loose	SG-condensed	SG-MIL-101(Cr)
Gluing rate (g/cm^2)	0.165	0.338	0.177*

*The gluing amount of SG-MIL-101(Cr) comes from the total weight/total area. The SG-MIL-101(Cr) composite desiccant is pre-mixed with a fixed ratio.

Table S2. Detailed information of IR images. Related to Figure 3.

Panel number - Time	Average T (℃)	Std. Dev. (℃)	Max/Min T (℃)
a – 0 min	25.8	0.3	26.5/24.8
a – 5min	37.7	1.5	40.1/32.8
a – 30min	40.3	2.7	43.3/33.8
b – 0 min	25.3	0.1	25.7/24.8
b – 5 min	56.7	3.4	62.3/44.8
b – 30 min	58.5	2.7	62.6/49.2
c – 0 min	24.7	0.2	25.5/24.2
c– 5min	47.0	1.9	50.7/40.4
c – 30min	55.8	3.3	60.7/44.5
d –0 min	24.9	0.1	25.4/24.4
d – 5 min	58.4	2.8	62.6/49.6
d – 30 min	60.6	2.2	64.0/52.6

*The emissivity is 0.9 and the detect distance is 1 meter.

Table S3. Adsorption and desorption rates for all the samples. Related to Figure 2 and Figure 5.

Sample	SG-MIL-101(Cr)	SG loose	SG condensed	Reference
Adsorption(s^{-1})	$1.02x10^{-4}$	$8.50x10^{-5}$	$5.95x10^{-5}$	$2.02x10^{-4}$
Desorption(s^{-1})	$5.41x10^{-4}$	$2.42x10^{-4}$	$2.47x10^{-4}$	$6.45x10^{-5}$

Table S4, Materials and costs involved in panel fabrication. Related to Figure 4.

Material	Amount	Total price (in RMB/USD)
PF	$0.01m^3$	10/1.5
SG(30 wt% silica-sol)	1.65kg(5.5kg)	50/7.5
Carbon black powder	10g	20/3
Cr(NO3)3	533g	30/4.5
H2BDC	220g	35/5.2
Solvents and electricity	-	25/3.7
Summary	-	170/25.5

* $Cr(NO_3)_3$ and H_2BDC are the row chemicals for MIL101(Cr) fabrication.

Transparent Methods

MIL101(Cr) synthesis. The synthesis of MIL101(Cr) was following the reported method(Ferey, 2005). The chromium (III) nitrate $Cr(NO_3)_3{\cdot}9H_2O$ (purchased from X) and H_2BDC (1,4-benzenedicarboxylic acid) were involved in the synthesis of MIL-101(Cr). 4.0g of chromium (III) nitrate and 1.66g H_2BDC were dispersed in 50mL of deionized (DI) water in a 100-mL stainless steel pressure vessel. The mixture was stirred for 10 minutes and consequently treated by ultra-sonic for 15 minutes to avoid aggregations. The pressure vessel was placed in an oven under a programmed heating-cooling process. The temperature rose from RT to 220℃ with a rate of 0.2℃/min, and was kept at 220℃ for 8 hours. Then cooling process is controlled at 0.2℃/min drop. Deep green suspension was acquired through this procedure. The SG-MIL101(Cr) composite desiccant was achieved by a pre-mix of MIL101(Cr) suspension and silica-sol in a controlled ratio (mass ratio of 1:10, see mass ratio control of the SG-MIL101(Cr)) and the mixed suspension is stirred overnight to ensure a total dispersion. The suspension was involved in the further steps (to form composite suspension with silica-sol)but MOF powders were also prepared for characterization such as dynamic water adsorption and nitrogen sorption (Figure S2)

Moisture permeable panel fabrication. The fabrication of moisture permeable panel can be divided into three major steps, including matrix pre-cleaning, desiccant layer formation and photo-thermal layer coating. The matrix foam was cut into 10cm*10cm pieces of panel with 1.0cm thickness. All the foam panels were thoroughly washed and dried to remove impurities. The loose layer was achieved by partially immerse the panel into silica-sol for 5 seconds. Similarly, the composite layer was obtained by immerse the panel into mixed suspension acquired above for 5 seconds. The condensed layer was obtained by multi-time immersion (3 times in this research). Then all panels were put into an oven under 65℃ for 24 hours. After the completion of desiccant layer, the surface was covered with nano size carbon black powder by suspension spraying method. The ethanol-water liquid mixture (1:4 in volume proportion) was introduced to reduce the hydrophobicity of CB powders. This liquid mixture can contribute a lot to the complete and

average dispersion of carbon black powder in the suspension. The suspension was prepared in a concentration of 0.1g/20mL. 10 minutes of shock and 15 minutes of ultra-sonic treatment are carried out to ensure the total and average dispersion. This suspension was put into a spray gun and 20mL of suspension was sprayed onto each panel surface (10cm*10cm). The panel was then placed in an oven under 65℃ for 4 hours. A water cleansing of the surface was introduced to remove the loosely attached carbon black powders (see Figure S4).

Water Vapor Transmission test. In the test of the Water Vapor Transmission experiment, a test dish, usually a beaker or a glass garden, was filled with controlled amount of distilled water and the specimen was attached to the test dish. The specimen was tightly sealed to the mouth of the test dish by aluminum foil and tapes to prevent any possible leakage. The water surface was controlled 19mm±6mm to the lower surface of the specimen, and the humid air above the liquid surface can be regarded as 100% relative humidity. This apparatus was placed in a temperature and humidity chamber to insure a constant environment outside the dish. An analytical balance was introduced to record the mass loss due to the water vapor difference between the two sides of the specimen. Sketch can be seen in Figure S5.

The sorption rate test

The dynamic adsorption (Figure S3a) and desorption (Figure S3b) measurements were carried out in the temperature-humidity constant room. All the samples were fully dried at 70℃ in an oven before adsorption under 25℃, 70%RH condition and all of them reached equilibrium at 25℃, 70%RH before desorption at 35℃, 70%RH, with one-sun illumination. The curves only present the performances of the first 3 hours which is critical for the dehumidification process. In adsorption process, the sample with SG-MIL-101(Cr) (red dots) achieves the best water uptake quantity (except the reference sample) while the sample with SG loose layer (blue triangles) only has a modest amount, demonstrating that the introduction of MIL-101(Cr) can largely improve the water uptake rate. The reference sample (black squares) has the same desiccant layer structure as the sample with SG loose layer, but very different water adsorption ability is observed. This is associated with the influence of PF foam which is introduced for thermal insulation, as described previously. The porous structure of PF foam, although accessible for water vapor transmission, clearly alleviates the water vapor transport ability and thus influence the water capture performance. However, identical equilibrium water adsorption quantity (0.181g/g) is acquired for both samples, indicating that the introduction of PF foam only reduces the water adsorption rate due to the tackle of the porous skeletons but scarcely influence the overall water uptake amount. In desorption process, the sample with SG-MIL-101(Cr) (red dots) losses water very fast while the reference sample (black squares) losses only a little. The surface temperature is considered as the dominating reasons. As illustrated in Figure S3, the IR images were taken to visualize the temperature distribution of the panels under one-sun illumination. The reference sample (a) and the CB coated sample (b) were both illuminated under one-sun condition and a temperature difference of 24℃ between the two samples are observed. The average temperature of (a) is around 38.2℃ while that of (b) can reach as much as 62℃. The side-view (c) clearly shows the temperature distribution along the normal vector of the panel surface. Steep temperature drop is observed ascribed to the excellent thermal insulation property of PF foam. The SG loose sample (blue triangles) and SG-condensed sample (green triangles) can desorb water much faster than the reference sample but still far from the SG-MIL-101(Cr) sample. This again shows the advantage of MIL-101(Cr) when losing water.

The LDF (linear driving force) model is applied to quantify the sorption rate [12]:

$$\frac{dx}{dt} = k(x - x_t) \quad (1)$$

where k stands for the rate coefficient (in s^{-1}), x for the equilibrium water uptake quantity (in g/g) and x_t for the dynamic water uptake quantity (in g/g). By combining eq. (1), the following equation is obtained:

$$-\ln\left(1 - \frac{x_t}{x}\right) = kt \quad (2)$$

The adsorption rate and desorption rate for all the samples are listed in Table S3.

The mass ratio control of the SG-MIL101(Cr)

The original MIL101(Cr) suspension was condensed to 0.1g/mL and was mixed with silica-sol (30% mass ratio) in a volumetric ratio of 3:5. Under such condition, the mass ratio of MIL101(Cr) and SG is 1:10. However, the addition of extra MIL101(Cr) suspension dilutes the silica sol, which may lead to a less mass ratio of the SG. Thus, the mixed suspension should be condensed again to re-gain the original mass-volume ratio of silica-sol. According to the volumetric ratio applied in the previous step, the volume of the condensed mixed suspension should be 62.5% that of the original mixed suspension.

Model and simulation

The carbon black powders are coated on the panel surface, and can convert the incident sunlight into heat via photo-thermal effect. Thus we can consider this layer as a surface heat source. The desiccant layer and PF layer are lying consequently under the carbon black layer with the same thickness of 0.5 cm. The left and right sides are considered as thermal insulated. (See Figure S6)
The thermal conductivity of PF layer is 0.035 $W \cdot m^{-1} \cdot K^{-1}$. The dominating equations are shown as follows:

$$q_{in} = q_{de} + q_{rad} + q_{cov} + q_{cod} + C_p m \frac{dT}{dt}$$

$$q_{in} = I_{in} * \eta$$

I_{in} stands for the intensity of incident sunlight, η the photo-thermal conversion efficiency.

$$q_{de} = \dot{m} * H$$

$\dot{m}$ stands for the desorption rate under illumination, H the phase change enthalpy of water.

$$q_{rad} = \varepsilon\sigma(T^4 - T_{amb}^4)$$

ε is the emittance of the carbon black surface. T and T_{amb} are surface and ambient temperatures, respectively. T_{amb} is set as 25°C according to the working condition.

$$q_{cov} = h(T - T_{amb})$$

$$q_{cod} = \lambda \frac{dT}{dx}$$

As the reviewer mentioned, two different situations should be considered: the desiccant layer is wet or partly dried. The thermal conductivities of each layer under two different conditions are measured: 0.08 $W \cdot m^{-1} \cdot K^{-1}$ when the desiccant is fully dried and 0.1 $W \cdot m^{-1} \cdot K^{-1}$ when the desiccant is wet under working condition. Besides, the q_{de} term also differs between two conditions: the water is desorbing very quickly when the layer is wet but becomes very slowly when the desiccant is dried. Therefore, the q_{de} term in wet layer is much larger than that of the dried layer. With a rough estimation, the q_{de} is set as 80 Wm^{-2} under wet condition and 10 Wm^{-2} under dried condition. The simulation results are shown in Figure S7 (only a zoomed-in area is shown for clearness).
From the results we can see that the temperature profiles of both conditions are similar and only a little difference is observed. Temperature of measurement points (on the interface between two

layers) are 334.16K for dry layer (a) and 332.72K for wet layer (b). Furthermore, the dry desiccant layer even has a higher temperature than the wet desiccant layer despite its lower thermal conductivity. This is mainly resulted from a much lower desorption rate which may consume a lot of heat. Therefore, although the desiccant is dried during the heating process and the thermal conductivity is reduced, the desiccant layer can still maintain an even higher temperature for continuous desorption.

Dehumidification rate:

The adsorption on the desiccant surface is usually expressed by following equation:

$$\frac{\partial W}{\partial t} = \frac{k}{\rho_d t_d}(Y_a - Y_d)$$

and inside the desiccant layer:

$$\frac{\partial(\rho_d W)}{\partial t} = \frac{\partial}{\partial z}[D_s \frac{\partial(\rho_d W)}{\partial z}]$$

Where W is the water uptake of the desiccant in g/g desiccant. ρ_d and t_d are the density and thickness of the desiccant. Y_a and Y_d stand for the water content of the ambient environment and in the desiccant, respectively, in g/kg air. D_s is the surface diffusion coefficient of water molecules inside the desiccant and k is the air-to-desiccant mass transfer coefficient.

In these equations, the W is connected with Y_d via the isotherms of the desiccant, and in fact, the W is strongly correlated with Y_d:

$$\mathrm{W} = W_d(\mathrm{T}, Y_d)$$
$$Y_d = f(T, W)$$

With a given temperature T, we can then obtain the W-Y_d relationship from the isotherms under this given temperature and the equation can be solved to obtain the W, which is exactly the water uptake of the desiccant during adsorption or desorption stage. The mass difference between the two stages can be considered as the humidity reduction amount and the humidity reduction rate can be consequently calculated.

$$r_{de} = \frac{\Delta W}{t_{cycle}}$$

Therefore, we can conclude from the above modeling that several parameters may influence the system performance. The water capacity of the desiccant W is an important parameter since it directly determines the adsorption quantity during each cycle. A larger adsorption quantity may lead to a higher humidity reduction rate. The mass transfer coefficients k and D_s are also dominating the performance. Larger coefficients may lead to higher adsorption quantity in the same adsorption period. The thermal conductivities of both desiccant layer and substrate (the PF layer in this paper) may also influence the system performance. On one hand, larger thermal conductivity of desiccant can lead to a higher-in-average temperature distribution in the desiccant layer, which may be helpful to the desorption process; On the other hand, a smaller thermal conductivity of substrate can prevent further heat loss by conduction via substrate, keeping more heat in the desiccant layer during desorption process.

Energy efficiency.

The energy efficiency η is 2.36%. But it should be noted that higher efficiency can be expected with rational improvements, e.g. new water capture material with much higher water capacity. Early this year (2019), Fei Zhao et.al.(Fei Zhao, 2019) reported a “super moisture-absorbent gels” which may potentially fulfill our needs. The PPy-Cl clusters aggregated on the gel matrix can

capture the water vapor in the air. Then the condensed water is transferred to the matrix (poly-NIPAM) for storage. Under 60% RH in room temperature, up to 3.4g/g water can be taken. This value is almost twice larger than that of MIL101Cr (~1.2g), and more than 5 times larger than that of SG (0.6g/g). If this super gel is applied, we can rationally expect a much larger water capacity of the panel with almost identical dimension, and consequently lead to a much better dehumidification rate. But since the lack of some related data (e.g. the isotherm under working condition, the permeability, the adsorption and desorption kinetics), it is difficult to quantitatively estimate the accurate values of potential efficiency currently.

Besides, the structure of the panel and the humidity pump, although have been optimized with our best, still has a great potential of improvements. Better mass transfer ability (permeability) can obviously accelerate the moisture transferring process and reduce the cycle period. If 20% enhancement of permeability is assumed, the cycle period can be reduced to 83% of what it originally is. This may lead to a 20% increase in dehumidification rate and consequently 20% higher in efficiency.

As we know, a conventional desiccant wheel solar dehumidification system may have a thermal COP around 0.4-0.6, but solar heating system as well as desiccant wheel air ducts should be installed, which could be another costive investment. Besides, such systems usually require manual control and frequent maintenance, and also occupy large spaces. This moisture penetrating humidity pump directly powered by one sun illumination has a simple structure and low cost, and may create a new insight for solar powered dehumidification.

Real world application:

Consider a department with area of 25 m^2(6.25 m length * 4 m width * 2.8 m height) with 1 inhabitant inside, the moisture load inside the department should be calculated as follows:

$$M_w = 0.001\varphi_B ng$$

φ_B stands for the assembly coefficient, n the number of inhabitant indoor and g the moisture release from an adult. Under such condition, 0.2kg/h of moisture load is introduced in this department. By using the best dehumidification rate we achieved in our paper, roughly 5.6 m^2 of such panels are needed to fully cover the moisture load, which equals to an area of 2.8m * 2m. This was based on the humidity pump operation period when sunshine is available. If we consider the moisture storage capability of the adsorbent layer, e.g. a moisture reservoir, a higher moisture adsorption capacity could be achieved, thus the humidity pump panel area could be further reduced.

We should mention that this moisture penetration humidity pump is only a proof-of-concept prototype, thus the results are not that competitive compared with the conventional dehumidification technologies. Several potential improvements may obviously increase the performance, including better desiccants with higher water capacity and moderate desorption temperature, optimized panel/pump structure with better mass transfer ability and thermal insulation, etc..

Besides, this humidity pump could also serve as a major dehumidifier to remove only part of the moisture load indoor instead of the whole. Under such condition, the efficiency of traditional AC system could be largely improved.

The performance-price ratio:

Since such humidity pump can directly utilize the solar illumination, metrics such as COP is not suitable for this system.

The fabrication of such panel involves several row materials and chemicals. Here we take 1 m^2 of such panel for the following calculation (see Table S4):

Please be noted that such costs are based on laboratory level, which can be largely decreased once it is industrially handled.

We can define a parameter PPR that can well describe the cost-performance relationship:

$$\text{PPR} = \frac{\text{unit price}}{r_{de}} = \frac{price}{1\ g\ (moisture\ load)/h}$$

Where unit price is the cost of panel with a certain area (1 m^2) in RMB(USD)/m^2, r_{de} the dehumidification rate of the panel with a certain area (1 m^2) in $gh^{-1}m^{-2}$. By using the data in our paper as well as the above mentioned total cost, the PPR of our humidity pump(HP) is PPR(HP)=5.0 RMB/1(g/h) (or 0.75 USD/1(g/h)). This value indicates that by achieving the ability to handle 1g of moisture load in 1 hour, the cost will be 5.0 RMB or 0.75 USD.

For comparison, a PV driven dehumidification system, which also utilize sunlight illumination as the energy source, is considered: The PV system receives sunlight and convert them into electricity. The generated electricity is then used for driving an AC system to remove the indoor moisture load. Typically, the COP of common AC system is around 3.0 which means by consuming 1J of electricity, 3J of heat load can be handled. Usually, 40% of the heat load is resulted from latent load or moisture load. Thus we can consider that by consuming 1J of electricity, 1.2J(=3J*40%) of moisture load is removed. The cost of solar PV module is usually around 8 RMB/1Wp. Using these parameters, we can obtain the PPR(PV) for a typical solar PV system:

$$1\text{g moisture load/h} = 2513\text{J moisture load/h} = 2094\text{J electricity/h}$$

$$\text{PPR(PV)} = \frac{8RMB}{1Wp} = \frac{8RMB}{3600J\ electricity/h} = \frac{8RMB}{1.71g\ moisture\ load/h} = 4.7RMB/1(g/h)$$

This shows that the solar PV system may cost 4.7RMB or 0.7 USD to achieve the ability to handle 1g moisture load in 1 hour. This cost is only slightly lower than that of our humidity pump system. However, this value only includes the solar PV system that generate electricity, the necessary pipes and air-conditioner are still not considered. It is hard to use the PPR parameter to value the pipes and air-conditioning facilities, but it is reasonable to estimate that the cost of solar PV-AC (PPR(PV-AC)) should be equal to or even higher than that of PPR(HP). Furthermore, it is still worthy to mention that the solar PV systems have been intensively studied for more than 30 years and increasing performance as well as the decreasing costs have been achieved. As above mentioned, this humidity pump is a new concept with very little optimization and improvements, and the costs are valued based on laboratory level rather than industrial level. We are confident, and also rational, to believe that our humidity pump may have a rising performance and falling cost with more detailed researches in the future.

References:

FEI ZHAO, G. Y. 2019. Super moisture absorbent geols for all weather atmospheric water harvesting. *Advanced Materials*.

FEREY, G. 2005. A chromium terephthalate-based solid with unusually large pore volumes and surface area (vol 309, pg 2040, 2005). *Science,* 310**,** 1119-1119.

KHUTIA, A., RAMMELBERG, H. U., SCHMIDT, T., HENNINGER, S. & JANIAK, C. 2013. Water Sorption Cycle Measurements on Functionalized MIL-101Cr for Heat Transformation Application. *Chemistry of Materials,* 25**,** 790-798.